J Fluoresc
DOI 10.1007/s10895-015-1688-9

ORIGINAL ARTICLE

Structurally Characterized Zn^{2+} Selective Ratiometric Fluorescence Probe in 100 % Water for HeLa Cell Imaging: Experimental and Computational Studies

Babli Kumari[1] · Sisir Lohar[1] · Milan Ghosh[1] · Sabyasachi Ta[1] · Archya Sengupta[2] · Prajna Paramita Banerjee[2] · Ansuman Chattopadhyay[2] · Debasis Das[1]

Received: 13 June 2015 / Accepted: 7 October 2015

Abstract Fluorescence recognition of Zn^{2+} in 100 % aqueous medium using 2-((1, 3 dihydroxy-2-(hydroxymethyl)propan-2 ylimino) methyl) phenol (SALTM) as ratiometric probe is reported. Moreover, SALTM can discriminate Zn^{2+} from Cd^{2+} very effectively. The binding constant and detection limit of the probe for Zn^{2+} is 2.2×10^{4} $M^{-1/2}$ and 2.79×10^{-8} M respectively. Interestingly, corresponding naphthalene derivative (HNTM) having less water solubility fails to be a ratiometric sensor. SALTM can detect intracellular Zn^{2+} in HeLa cervical cancer cells under fluorescence microscope. Moreover, DFT and TD-DFT studies support experimental findings.

Keywords Zn2+ · Ratiometric · Fluorescence · HeLa cell imaging · Computational studies

Introduction

As second most abundant metal ion in human body after iron, zinc plays vital role in numerous biological processes, including brain activity, gene transcription, and immune function [1, 2]. In addition, disruption of Zn^{2+} homeostasis may be implicated in a number of severe neurological diseases like Alzheimer's & Parkinson's diseases, amyotrophic lateral sclerosis, hypoxia ischemia, and epilepsy [2–13]. Therefore, recognition and determination of Zn^{2+} in living tissues is a subject of great importance [1, 2, 14] and attracted immense interest in chemical and biological sciences. Fluorescence recognition of Zn^{2+} has paramount importance as it does not provide any spectroscopic or magnetic signals [2, 15–18]. According to the World Health Organization (WHO), the maximum acceptable level of Zn^{2+} in drinking water is 76 μM. Hence, selective recognition of Zn^{2+} is very important in supramolecular chemistry [19]. Recently, considerable efforts have been observed for in vitro and in vivo detection of Zn^{2+} [20–24]. Most of them are based on quinoline, anthracene, coumarin, BODIPY, and fluorescein fluorophores [25–32]. However, most of them involve complicated syntheses/hazardous reaction conditions and expensive chemicals/reagents. Some have poor water solubility/ interference from same group cations [33–36], limiting their real applications. Thus, interference free Zn^{2+} sensor that functionsin fully aqueous medium [37] for real applicationsis highly demanding. Schiff bases [31, 32, 38–40] incorporating a fluorescent unit are appealing reagents for optical sensing of metal ions [38–42]. Furthermore, most of the sensors exhibit only changes of emission intensity at a single wavelength which may be misleading due to several environmental factors. This may be eliminated through ratiometric fluorescence sensing and hence, more desirable [43, 44]. All these facts have inspired us to designa very simple, highly

CCDC numbers of SALTM and HNTM are 992217 and 993440 respectively.

✉ Debasis Das
ddas100in@yahoo.com

[1] Department of Chemistry, The University of Burdwan, Burdwan, West Bengal, India

[2] Department of Zoology, Visva Bharati University, Santiniketan, West Bengal, India

Published online: 20 October 2015

Scheme 1 Synthesis of SALTM and HNTM

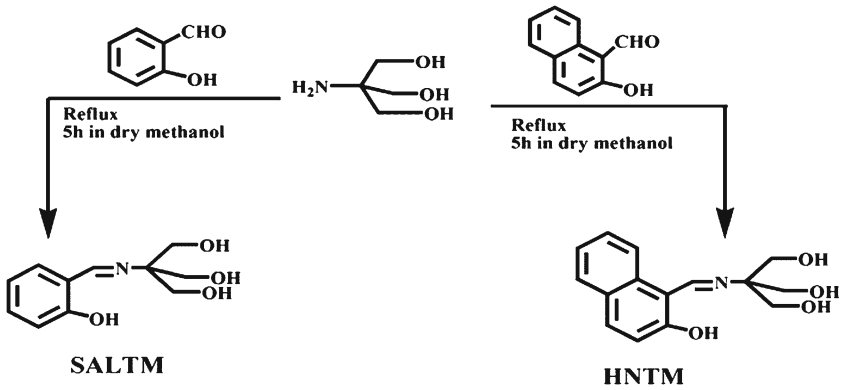

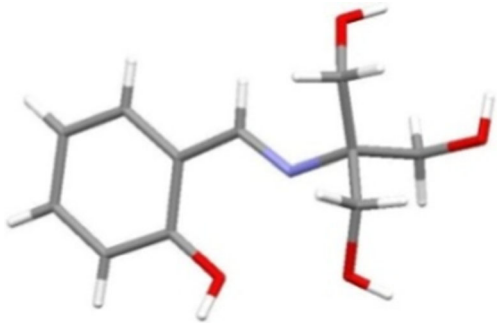

Fig. 1 Single crystal X-ray structure of SALTM

sensitive and Zn^{2+}selective ratiometric fluorescence sensor, SALTM that operates in 100 % aqueous solution. SALTM is prepared from salicyldehyde and tris(hyrdoxymethyl)amino methane as shown in Scheme 1. Replacing salicyldehyde by 2-hydroxy naphthaldehyde generates a model compound, HNTM that does not behave ratiometrically, however normal turn on Zn^{2+} sensing is observed. A similar probe to that of HNTM where amino methanol units are replaced by aminoethanol units, also functions as a normal turn on Zn^{2+} sensor [45]. To the best of our knowledge,

Fig. 2 ^{1}H NMR spectrum of SALTM in DMSO-d_6

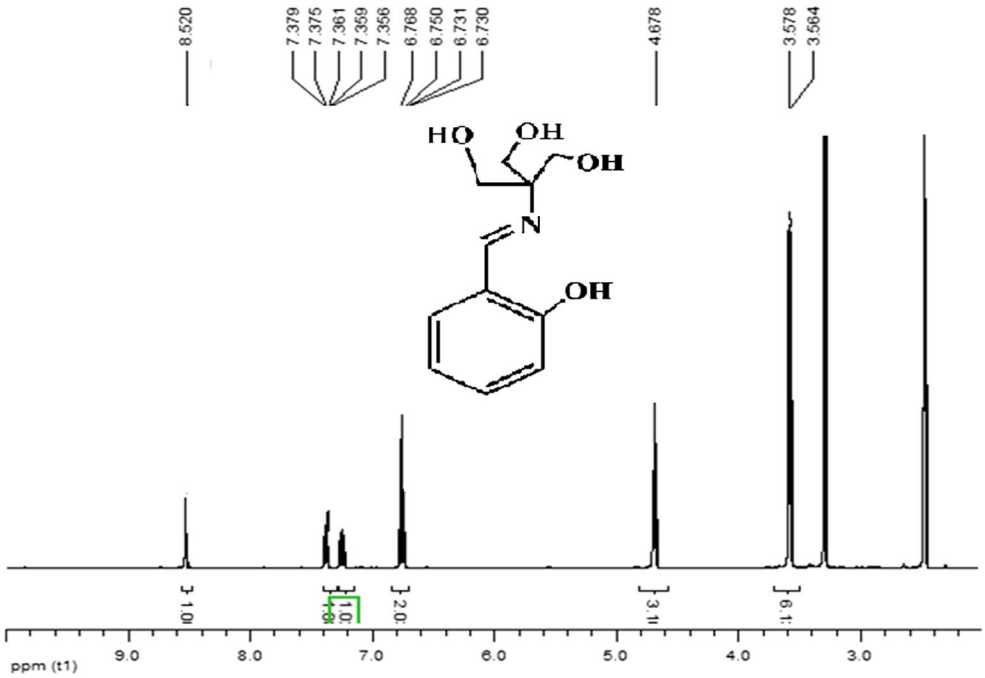

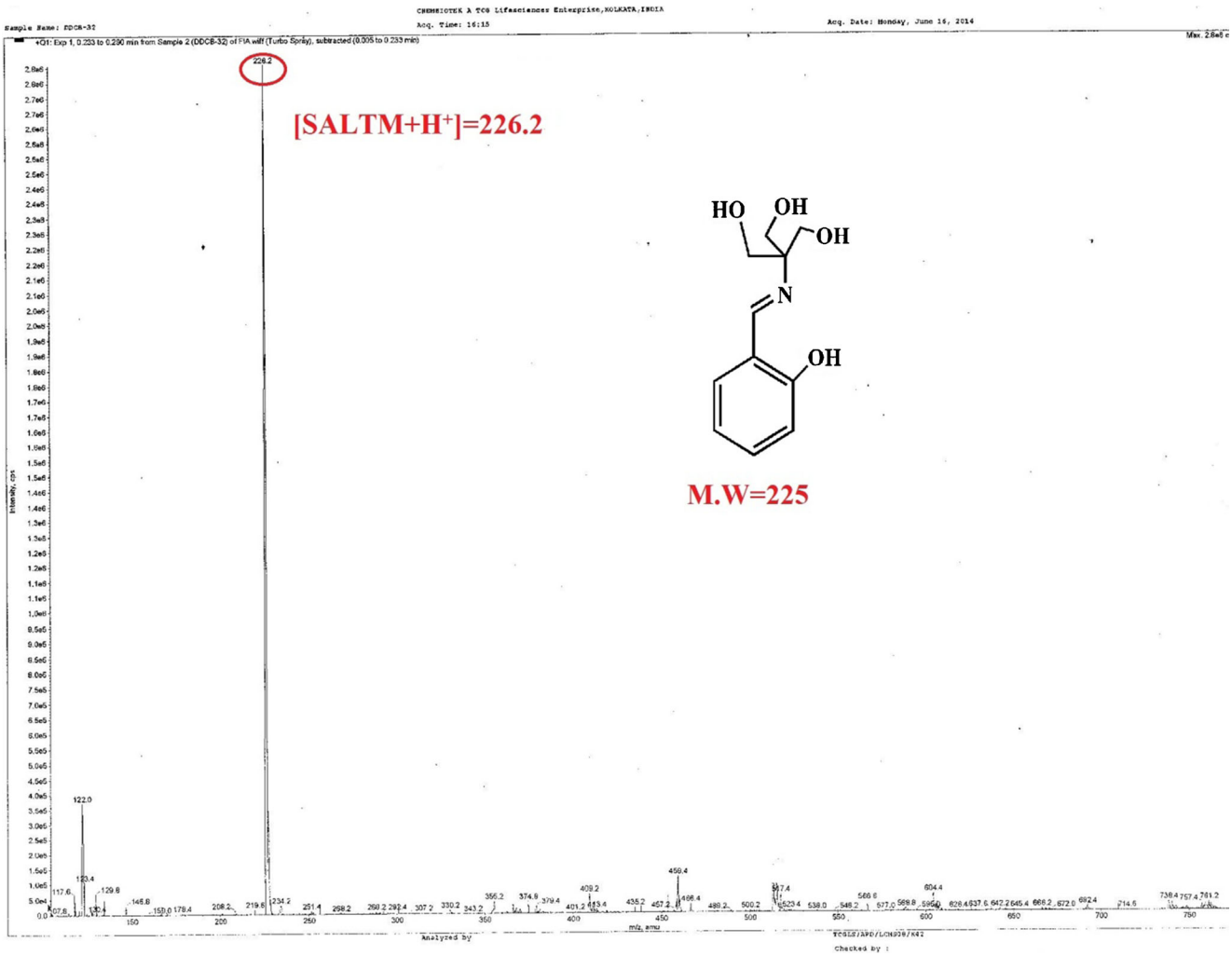

Fig. 3 QTOF mass spectrum of SALTM

SALTM is the first ratiometric Zn^{2+} sensor in 100 % water. HeLa cell comprises an immortalized, continuously cultured cell line of human cancer cells. Unlike normal body cells, HeLa cells thrive indefinitely in laboratory tissue culture, a trait that has made them important in research work. Fluorescence cell imaging of intracellular Zn^{2+} is performed in HeLa cells [46, 47].

Experimental

General Procedure

High-purity HEPES, tris(hydroxylmethyl)amino methane, salicyldehyde and 2-hydroxy napthaldehyde have been purchased from Sigma Aldrich (India). $Zn(OAc)_2.2H_2O$ is purchased from Merck (India). Solvents used are of spectroscopic grade. All other chemicals are of analytical grade and used without further purification. Mili-Q Milipore® 18.2 MΩ cm^{-1} water is used in experiments. Shimadzu UV–Vis-2450 spectrophotometer is used for recording absorption spectra. FTIR spectra are recorded on a Shimadzu FTIR spectrometer. Mass spectra are performed on a QTOF Micro YA 263 mass spectrometer in ES positive mode [1].H NMR spectra are recorded with Bruker Avance 600 (600 MHz) spectrometer. Solution pH is measured with Systronics digital pH meter (model 335). HCl or NaOH (50 mM) is used for pH adjustment. The steady-state fluorescence spectra are recorded with a Hitachi F-4500 spectrofluorimeter. The fluorescence microscope imaging system is composed of an inverted fluorescence microscope (Dewinter, Italy). Images are captured with an attached

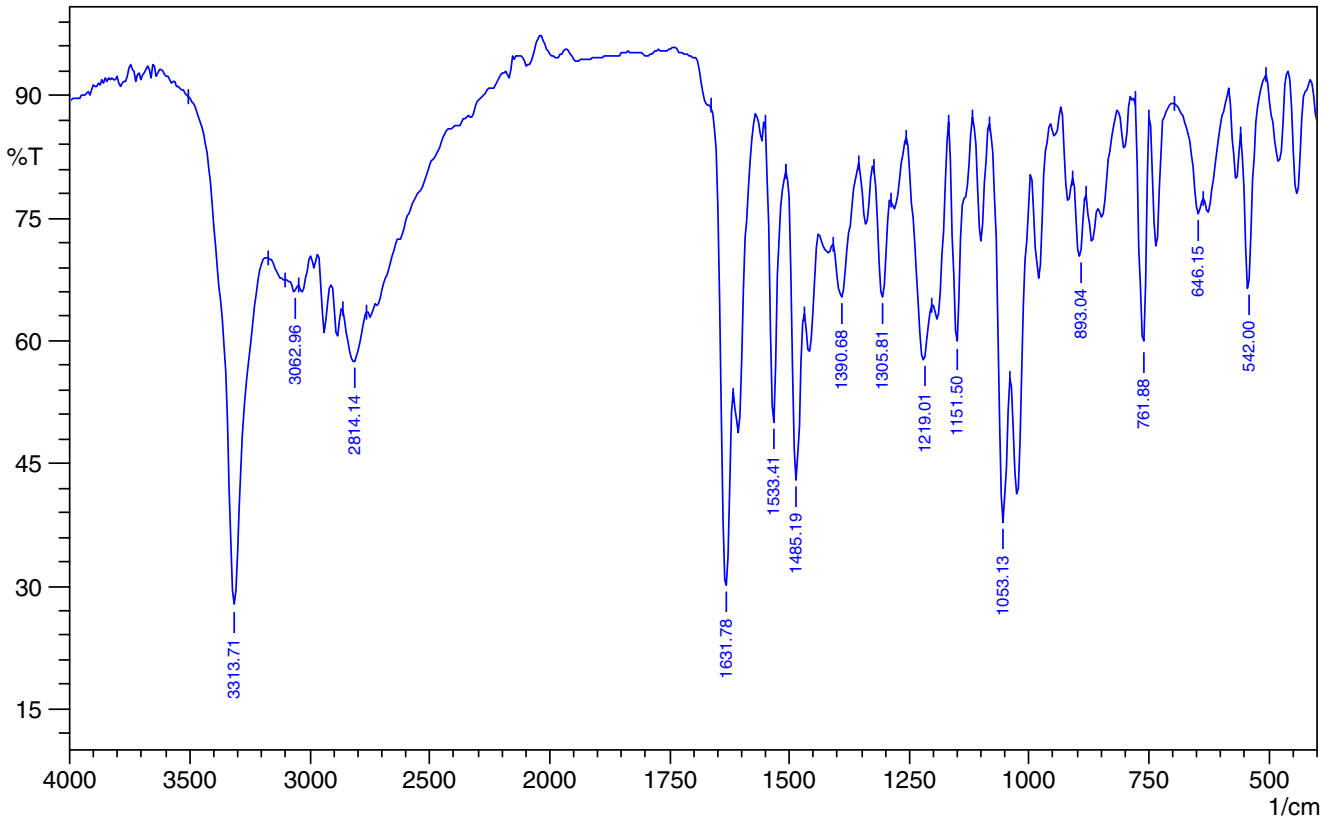

Fig. 4 FTIR spectrum of SALTM

CCD camera and processed with BioWizard 4.2 software. The microscope is equipped with a 50 W mercury arc lamp.

Synthesis of 2-((1, 3-dihydroxy-2-(hydroxymethyl)propan-2ylimino)methyl)phenol(SALTM) SALTM is synthesized as shown in Scheme 1. Methanol solution of salicylcadehyde (250 mg, 2.05 mmol, 10 mL) is added to tris(hydroxymethyl)amino methane (248 mg, 2.05 mmol, 25 mL) in methanol. The mixture is refluxed for 5 h. Slow evaporation of the solvent produces yellow crystals of the receptor in 91 % yield (420 mg). The structure of the receptoris established by single crystal X-ray structure (Fig. 1).^{1}H NMR (Fig. 2,) (600 MHz, DMSO-d_6), δ (ppm): 8.52 (1H, S), 7.37 (1H, d, J=2.4Hz),7.35 (1H, t, J=1.2Hz), 7.23 (2H, m, J=10.8Hz), 3.57 (6H, d, J=8.4); ESI MS (Fig. 3): $[SALTM+H]^{+}$=226.2; FTIR (cm^{-1}) (Fig. 4): υ(O-H phenol) 3313, υ(C=O ketone) 1631, υ(CH=N) 1595.

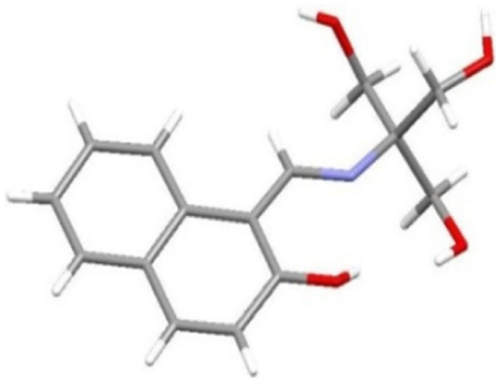

Fig. 5 Single crystal X-ray structure of HNTM

Synthesis of 1-((1,3dihydroxy-2-(hydroxymethyl)propan-2-ylimino)methyl)naphthalene-2-ol(HNTM) Scheme 1 shows the synthetic pathway for HNTM. Methanol solution of 2-hydroxy napthaldehyde (250 mg, 1.45 mmol, 10 mL) is added to dry methanol solution of tris(hydroxymethyl)amino methane (176 mg, 1.45 mmol, 25 mL). The mixture is refluxed for 5 h. Slow evaporation of the solvent generates yellow crystals of HNTM in 87 % yield (350 mg). The structure of HNTM has been established by single crystal X-ray strcuture (Fig. 5).

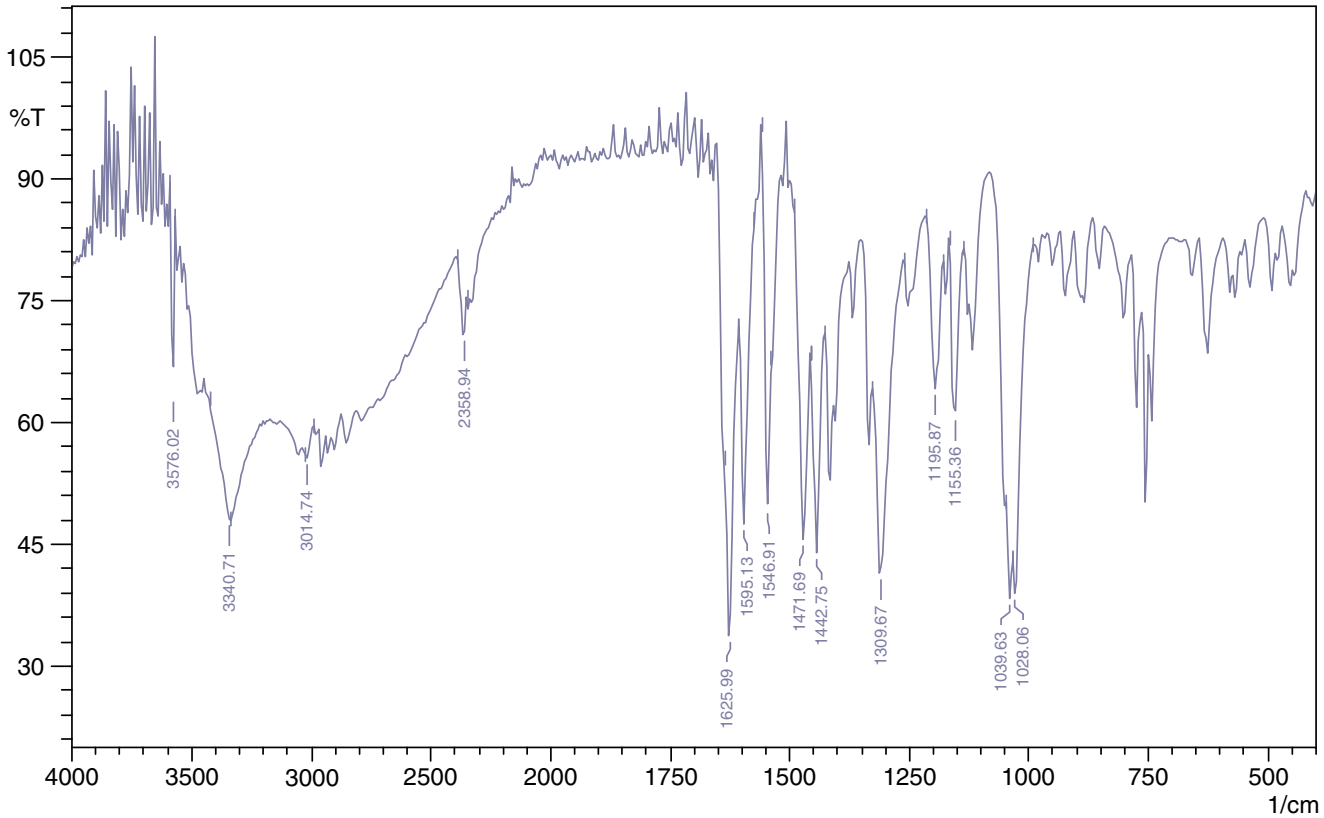

Fig. 6 FTIR spectrum of SALTM-Zn^{2+} complex

Synthesis of [Zn^{2+}-SALTM-H]adduct

10 mL methanol solution of $Zn(OAc)_2.2H_2O$ (87.6 mg, 0.4 mmol) is added slowly to the magnetically stirred solution of SALTM (90 mg, 0.4 mmol, 10 mL) in dry methanol. The mixture is stirred for 30 min and kept at room temperature for few days to get white crystalline [SALTM-Zn^{2+}] adduct. FTIR (cm^{-1}), (Fig. 6): υ(O-H, phenol), 3340; υ(C=O, ketone), 1625, υ(C=N), 1595. The ESI-MS spectrum (Fig. 7) of [SALTM-Zn^{2+}] adduct shows peak at m/z, 513 which clearly confirms the adduct formation.

Single Crystal X-ray Structure Analysis

Diffraction data for SALTM and HNTM are collected at 296[2] K on a Bruker SMART 1000 CCD diffractometer using graphite-monochromated Mo-Kα radiation (λ= 0.71073 Å). Some significant crystal parameters and refinement data are summarized in Tables 1, 2, 3, 4, 5 and 6. Data are processed and corrected for Lorentz polarization effects. Multi-scan absorption corrections have been performed using SHELXL-2013(Sheldrick, 2013) program. The structure is solved by standard direct methods [48] and refined by full matrix least squares on F^2 [49].

Cytotoxicity Assay

In vitro cytotoxicity is measured using the colorimetric methyl thiazolyltetrazolium (MTT) assay against Hella cells. Cells are seeded into 24-well tissue culture plate in presence of 500 mL Dulbecco's modified eagle medium (DMEM) supplemented with 10 % fetal bovine serum (FBS) and 1 % penicillin/streptomycin at 37 °C and 5 % CO_2 atmosphere for overnight and then incubated for 48 h in presence of SALTM at different concentrations (10–100 mM). Then cells are washed with PBS buffer and 500 mL supplemented DMEM medium is added. Subsequently, 50 mL MTT (5 mg mL^{-1}) is added to each well and incubated for 4 h. Next, violet formazan is dissolved in 500 mL sodium dodecyl sulfate solution in water–DMF mixture. The absorbance of solution is measured at 558 nm using microplate reader. The cell viability is determined assuming 100 % cell viability for cells without SALTM.

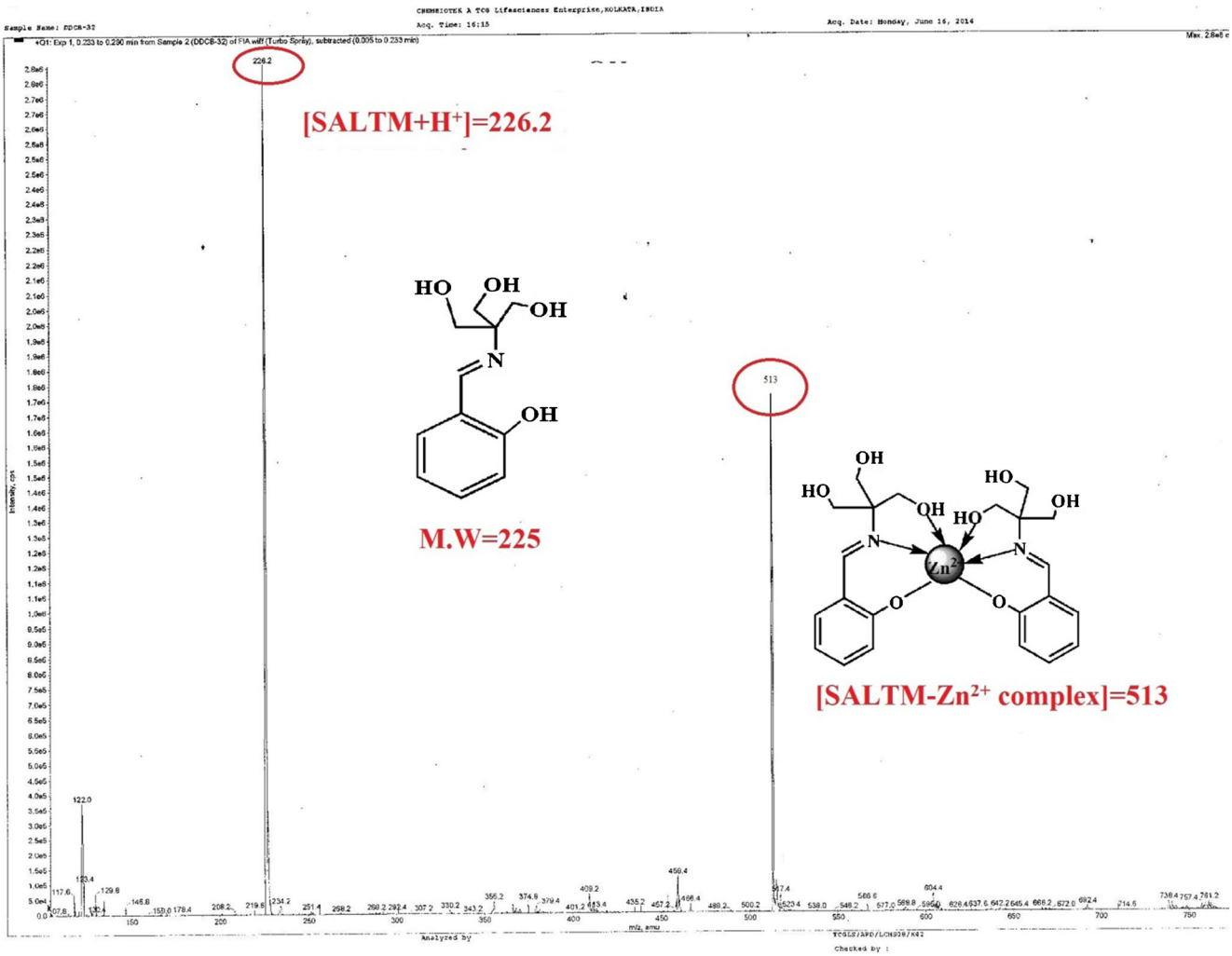

Fig. 7 QTOF mass spectrum of [SALTM-Zn^{2+}] complex

Table 1 Crystal parameters for SALTM

Identification code	SALTM
Chemical formula	$C_{11}H_{15}NO_4$
Formula weight	225.24
Temperature	296(2) K
Wavelength	0.71073 Å
Crystal system	Monoclinic
Space group	P 1 21/c 1
Unit cell dimensions	a=10.5261(4) Å, b=8.7390(3) Å, c=12.6573(4) Å
	α=90°, β=101.6120(15)°, γ=90°
Volume	1140.48(7) $Å^3$
Z	4
Density (calculated)	1.312 g/cm^3
Absorption coefficient	0.100 mm^{-1}
F(000)	480

Results and Discussion

SALTM and HNTM have been synthesized following Schemes 1 and 2. Single crystals of SALTM and HNTM are grown from methanol solution and

Table 2 Bond lengths (Å) of SALTM

O(001)-C(007)	1.2970(18)	O(002)-C(00B)	1.4141(18)
O(003)-C(00D)	1.417(2)	N(004)-C(008)	1.2978(19)
N(004)-C(009)	1.4790(17)	O(1)-C(00C)	1.419(2)
C(006)-C(00A)	1.415(2)	C(006)-C(008)	1.423(2)
C(006)-C(007)	1.4329(19)	C(007)-C(00 F)	1.418(2)
C(009)-C(00C)	1.5285(19)	C(009)-C(00D)	1.538(2)
C(009)-C(00B)	1.539(2)	C(00A)-C(00E)	1.365(2)
C(00E)-C(00G)	1.402(3)	C(00 F)-C(00G)	1.372(3)

Table 3 Bond angles (°) for SALTM

C(008)-N(004)-C(009)	127.70(12)	C(00A)-C(006)-C(008)	118.93(13)
C(00A)-C(006)-C(007)	119.99(13)	C(008)-C(006)-C(007)	121.03(13)
O(001)-C(007)-C(00 F)	122.19(13)	O(001)-C(007)-C(0060	121.17(13)
C(00 F)-C(007)-C(006)	116.64(13)	N(004)-C(008)-C(006)	123.38(13)
N(004)-C(009)-C(00C)	111.95(12)	N(004)-C(009)-C(00D)	106.08(11)
C(00C)-C(009)-C(00D)	108.06(13)	N(004)-C(009)-C(00B)	106.58(11)
C(00C)-C(009)-C(00B)	113.14(12)	C(00D)-C(009)-C(00B)	110.82(12)
C(00E)-C(00A)-C(006)	121.54(14)	O(002)-C(00B)-C(009)	111.50(12)
O(1)-C(00C)-C(009)	114.08(13)	O(003)-C(00D)-C(009)	112.29(13)
C(00A)-C(00E)-C(00G)	118.73(15)	C(00G)-C(00 F)-C(007)	121.51(15)
C(00 F)-C(00G)-C(00E)	121.53(15)		

Table 4 Crystal parameters of HNTM

Identification code	HNTM
Chemical formula	$C_{15}H_{17}NO_4$
Formula weight	275.29
Temperature	296(2) K
Wavelength	0.71073 Å
Crystal system	Monoclinic
Space group	P 1 21/c 1
Unit cell dimensions	a=21.131(5) Å, b=5.9906(12) Å, c=10.662(2) Å
	α=90°, β=92.077(15)°, γ=90°
Volume	1348.8(5) $Å^3$
Z	4
Density (calculated)	1.356 g/cm^3
Absorption coefficient	0.099 mm^{-1}
F(000)	584

Table 5 Bond lengths (Å) of HNTM

O(001)-C(00B)	1.413(7)	O(002)-C(008)	1.427(6)
O(003)-C(00E)	1.413(7)	O(004)-C(00A)	1.423(6)
N(005)-C(007)	1.304(6)	N(005)-C(006)	1.486(6)
C(006)-C(00A)	1.523(7)	C(006)-C(008)	1.532(7)
C(006)-C(00B)	1.540(7)	C(007)-C(009)	1.410(7)
C(009)-C(00E)	1.429(7)	C(009)-C(00D)	1.454(7)
C(00C)-C(00D)	1.412(7)	C(00C)-C(00G)	1.418(7)
C(00C)-C(00H)	1.438(8)	C(00D)-C(00 F)	1.367(7)
C(00E)-C(00I)	1.445(7)	C(00 F)-C(00 J)	1.367(7)
C(00G)-C(00 K)	1.363(9)	C(00H)-C(00I)	1.348(8)
C00J-C00K	1.375(8)		

characterized by X-ray crystallography (Figs. 1 and 2). The most significant geometric data are shown in Tables 1, 2, 3, 4, 5 and 6.

As pH of the medium may affect the charge distribution of the receptor, specially having acidic donor site, and consequently influence its indigenous emission properties, optimization of pH have been performed to monitor the emission characteristics of SALTM and its Zn^{2+} complex.

Figure 8 shows poor sensing abilities of SALTM for Zn^{2+} at pH below 6, probably due to protonation of the donor centers. However, SALTM recognizes Zn^{2+} over a wide range of pH from 6.0 to 11.0. Two pKa [50] values for SALTM, viz. 5.06 (for

Table 6 Bond angles (°) of HNTM

C(007)-N(005)-C(006)	126.9(4)	N(005)-C(006)-C(00A)	113.9(4)
N(005)-C(006)-C(008)	105.7(4)	C(00A)-C(006)-C(008)	111.4(4)
N(005)-C(006)-C(00B)	106.6(4)	C(00A)-C(006)-C(00B)	107.5(4)
C(008)-C(006)-C(00B)	111.7(4)	N(005)-C(007)-C(009)	123.3(5)
O(002)-C(008)-C(006)	109.8(4)	C(007)-C(009)-C(00E)	119.2(4)

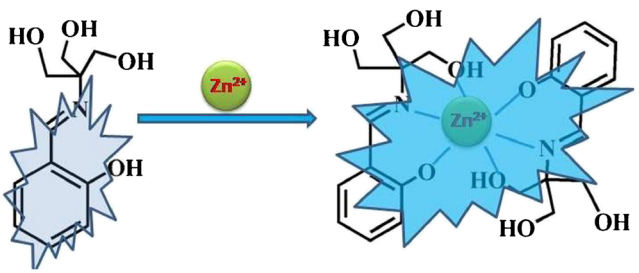

Scheme 2 Proposed binding mechanism of SALTM to Zn^{2+}

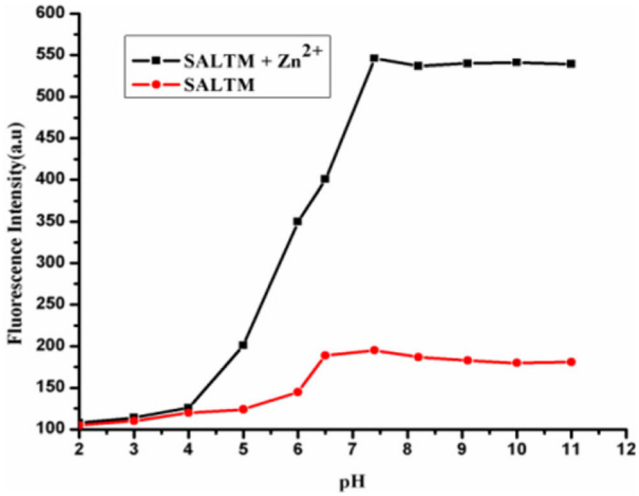

Fig. 8 Effect of pH on the emission intensities of SALTM (20 μM) and SALTM-Zn^{2+} adduct

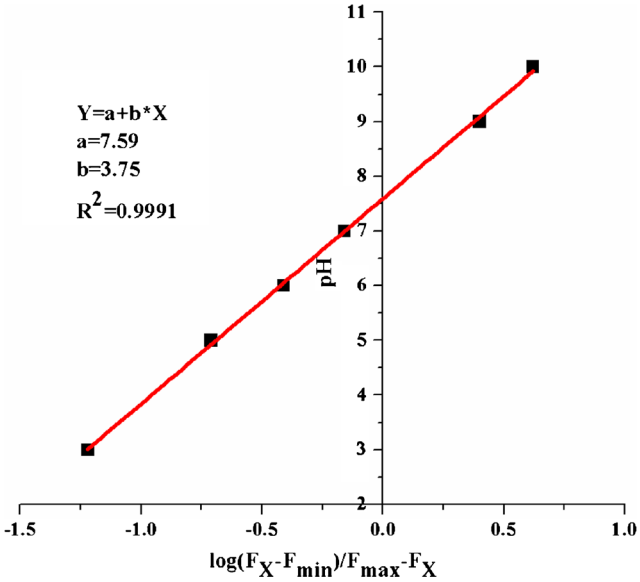

Fig. 10 Determination of pKa2 of SLTM using fluorescence method (λ_{Em}, 450 nm)

pKa1 at acidic pH, Fig. 9) and 7.59 (for pKa2 at basic pH, Fig. 10) indicate that its sensing ability is higher around neutral pH. However, difference in the emission intensities between SALTM and its Zn^{2+} adduct is highest at pH 7.4. SALTM shows weak emission centered at 370 nm (λ_{ex}=300 nm) with a low quantum yield, 0.012. In presence of different common cations, viz. Na^{+}, K^{+}, Ca^{2+}, Mn^{2+}, Mg^{2+}, Hg^{2+}, Co^{2+}, Ni^{2+}, Cu^{2+}, Pb^{2+}, Fe^{2+}, Zn^{2+} and Cd^{2+}, significant change in emission properties is observed in presence of Zn^{2+} (Fig. 11). Addition of Zn^{2+} to the aqueous solution of SALTM reduces the emission intensity at 370 nm while a sharp fluorescence enhancement is observed at 450 nm. Thus a ratiometric fluorescence change is observed with a sharp iso-emissive point at 381 nm, demonstrating the existence of equilibrium in solution (Fig. 12). The intensity ratio, $F_{450\ nm}/F_{370\ nm}$ exhibits a sigmoid curve against the added Zn^{2+} (Fig. 13a). The fluorescence quantum yield of the adduct increases more than 6-fold compared to that of free probe having value, 0.073.

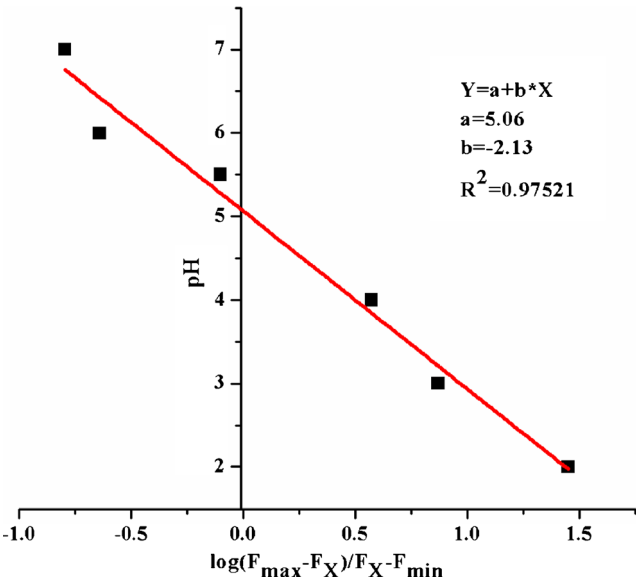

Fig. 9 Determination of pKa1 of SALTM using fluorescence method (λ_{Em}, 450 nm)

SALTM has another excitation at 370 nm. Interestingly, excitation at this wavelength in presence of Zn^{2+} results normal fluorescence enhancement at 450 nm. As Zn^{2+} selective ratiometric fluorescence probe functioning in fully aqueous medium is very rare, we have opted the ratiometric protocol for Zn^{2+} sensing.

Calculation of Quantum Yield

Fluorescence quantum yields (Φ) are estimated by integrating the area under the fluorescence curves using the equation,

$$\phi_{\text{sample}} = \frac{\text{OD}_{\text{standard}} \times A_{\text{sample}}}{\text{OD}_{\text{sample}} \times A_{\text{standard}}} \times \phi_{\text{standard}}$$

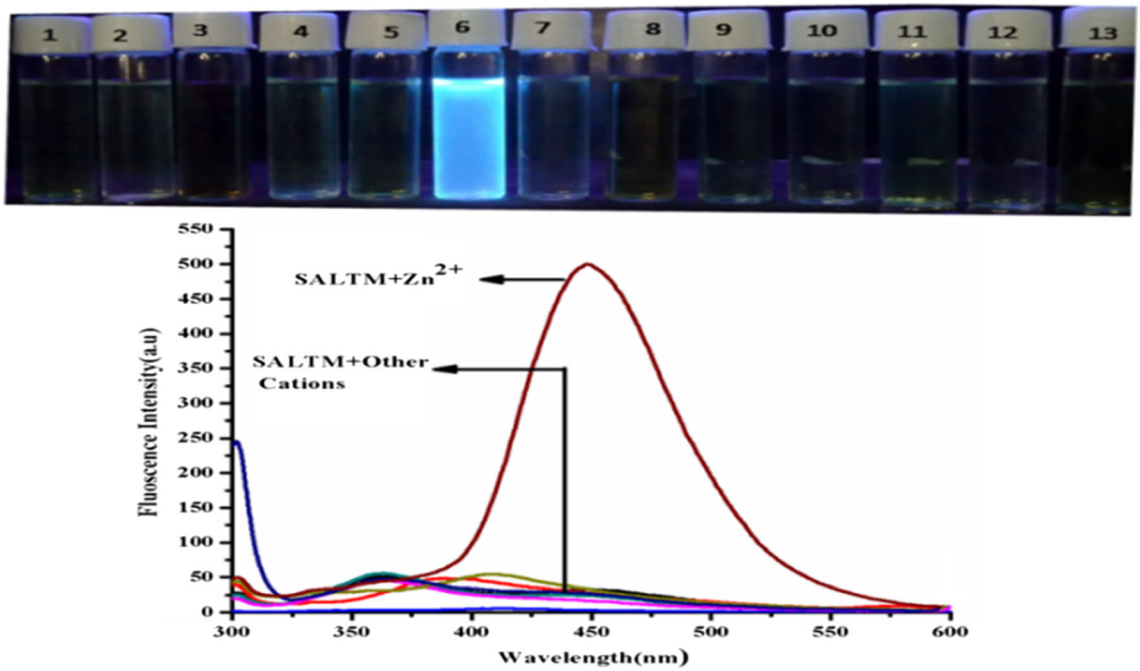

Fig. 11 Relative emission intensity of SALTM (20 μM) in presence of different metal ions (100 μM) in aqueous solution(0.1 M, pH 7.4), λ_{ex}= 300 nm, λ_{em}=450 nm (*bottom*). UV light exposed color of SALTM in presence of different cations; Mn^{2+} (1), Cd^{2+} (2), Ni^{2+} (3), Co^{2+} (4), Mg^{2+} (5) Zn^{2+} (6), Hg^{2+} (7), Cu^{2+} (8), Ca^{2+} (9), Pb^{2+} (10), Fe^{3+} (11), Fe^{2+} (12), Pb^{2+} (13) (*top*)

where A is the area under the fluorescence spectral curve and OD is optical density of the probe at the excitation wavelength [51]. Anthracene is used as quantum yield standard (quantum yield 0.27 ethanol) [52] for measuring the quantum yields of the probe and its Zn^{2+} complex.

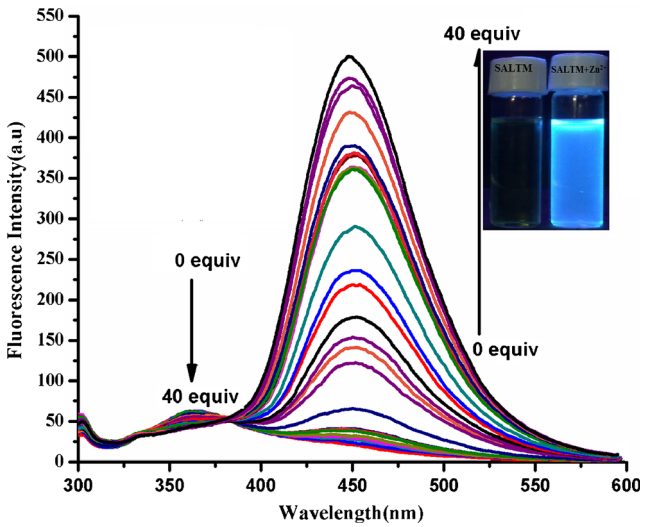

Fig. 12 Changes in the emission spectra of SALTM (20 μM) in 100 % water at pH 7.4 upon gradual addition of Zn^{2+} (0.1, 0.2, 0.5, 1.0, 2.0, 3.0, 4.0, 5.0, 6.0, 7.0, 8.0, 9.0, 10.0, 25.0, 50.0, 100.0, 200.0, 400.0, 600.0 and 800.0 μM), λ_{ex}=300 nm. (Inset: UV light exposed color change of SALTM upon addition of Zn^{2+}

Plot of the emission intensity vs. externally added Zn^{2+} generates a sigmoid graph (Fig. 13b) having linearity up to 100 μM Zn^{2+}, useful for determination of unknown Zn^{2+} concentration. The fluorescence enhancement is attributed to the formation of a rigid system upon binding of the probe to Zn^{2+}, restricting CH=N isomerization leading to chelation-enhanced fluorescence (CHEF).

The detection limit [53] is calculated from the fluorescence titration (Fig. 14). To determine the S/N ratio, the emission intensity of SALTM without Zn^{2+} is repeated 10 times from which the standard deviation of blank is determined. The detection limit is then calculated using the equation: DL=3×SD/S, where SD is the standard deviation of the blank and S is the slope of the calibration curve. From the graph, the values for Sand SD are 2.7484is 0.0256. Thus, the detection limit (DL) is 2.79×10^{-8} M.

Corresponding naphthalene derivative, the model compound, HNTM has low water solubility and recognize Zn^{2+} via normal turn on mechanism. A similar Zn^{2+} sensor to that of HNTM have reported the same observations [45].

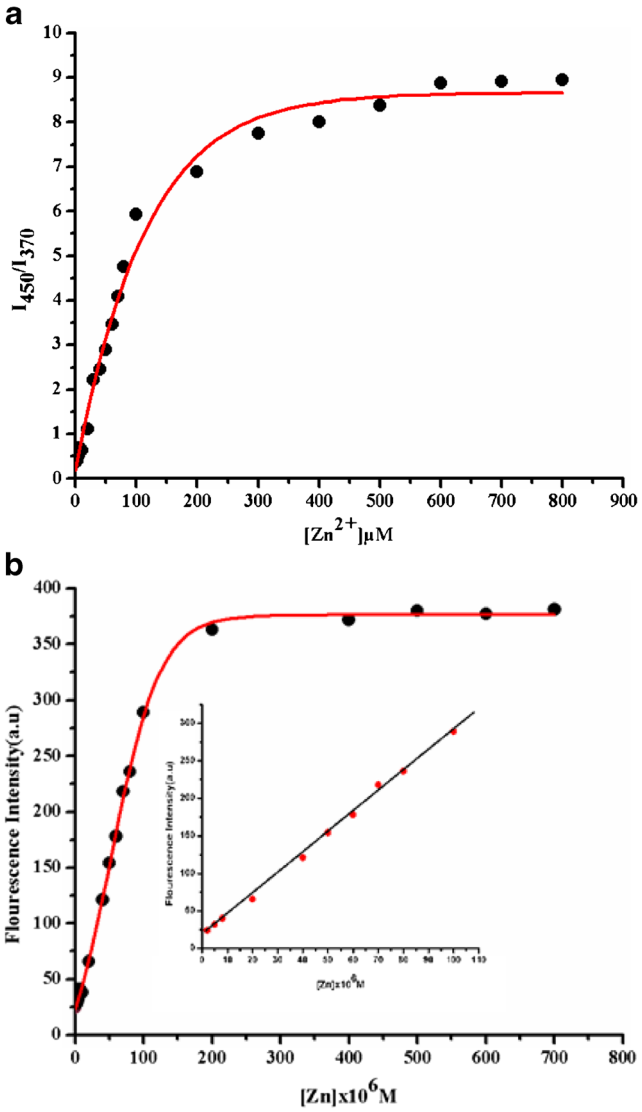

Fig. 13 **a** Ratiometric calibration curve, $I_{450\ nm}/I_{370\ nm}$ as a function of Zn^{2+} concentration (λ_{Ex}=300 nm). **b** Emission intensity vs. externally added Zn^{2+} (0.1–800.0 μM) of SALTM (λ_{Ex}=300 nm)

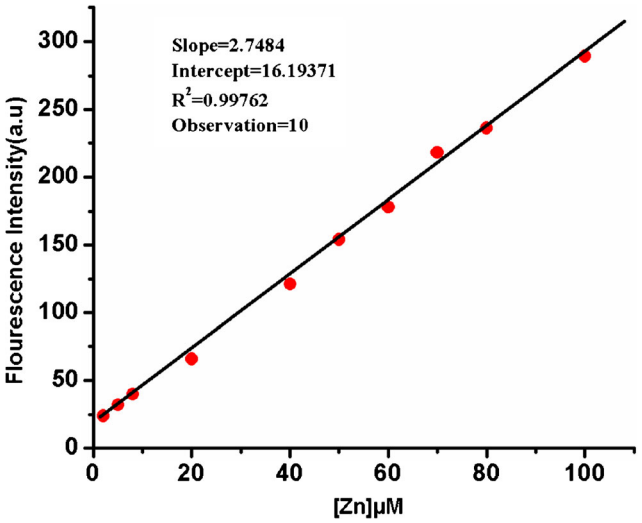

Fig. 14 Emission intensity vs. externally added Zn^{2+} of SALTM (λ_{Ex}= 300 nm) for calculation of detection limit

Job's plot (Fig. 15) shows the stoichiometry of SALTM –Zn^{2+} complex as 2: 1 (mole ratio). A competitive experiment with different metal ions indicates that most of the 3d and bio-relevant cations do not interfere significantly (Fig. 16). The binding constant of SALTM for Zn^{2+} is 2.2×10^4 $M^{-1/2}$, obtained using Benesi-Hildebrand equation [54], F_{lim}-F_0/ F_X-F_0=1+(1/K[C]^n) where, F_0, F_x, and F_{lim} are the emission intensities of the probe in absence of Zn^{2+}, at an intermediate Zn^{2+} concentration, and at a concentration of the complete interaction with Zn^{2+} respectively. K is the binding constant, C is the concentration of Zn^{2+} and n is the number of Zn^{2+} ions bound per SALTM molecule (here, n=1/2) (Fig. 17).

On the other hand, fluorescence titration of HNTM with Zn^{2+} (Fig. 18) in HEPES buffer (pH 7.4, λ_{ex}= 380 nm, λ_{em}=450 nm) indicates normal turn on fluorescence behaviour.

The absorbance of aqueous solution of SALTM (pH 7.4) at 400 nm (Fig. 19) gradually decreases upon

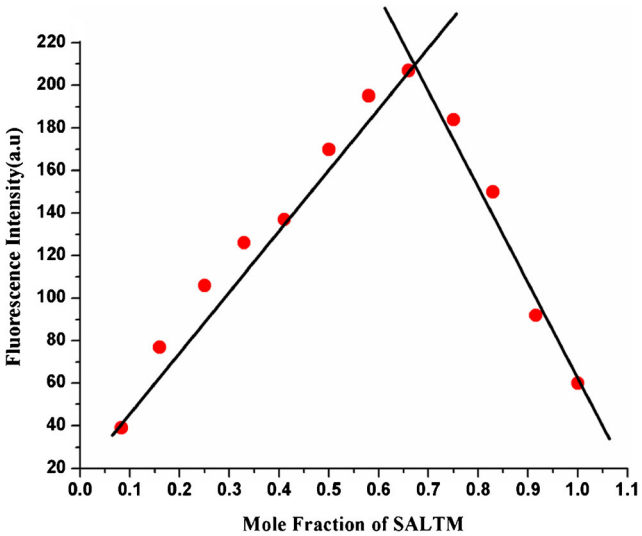

Fig 15 Job's plot for the determination of stoichiometry of [SALTM-Zn^{2+}] complex in 100 % water at pH 7.4 (λ_{ex}=300 nm, λ_{em}=450 nm)

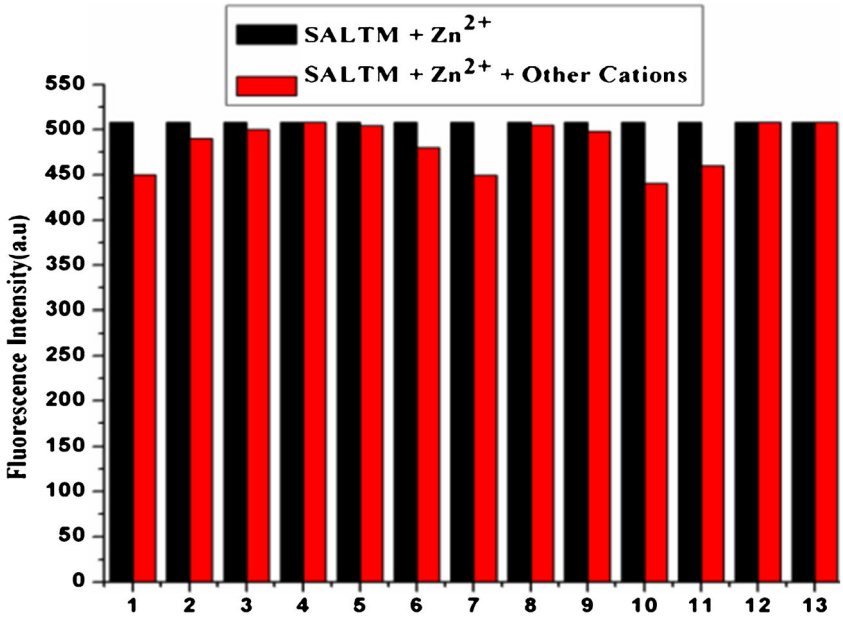

Fig. 16 Relative emission intensities of SALTM-Zn^{2+} system in presence of various cations in 100 % water at pH 7.4. *Black bars* represent the emission intensity of the [SALTM-Zn^{2+}] system and *red bars* show the emission intensity of the [SALTM-Zn^{2+}] system in presence of 100 equiv. of different cations, viz. Cu^{2+} (1), Mn^{2+} (2), Cd^{2+} (3), Mg^{2+} (4), Hg^{2+} (5), Cr^{3+} (6), Ni^{2+} (7), Al^{3+} (8), Pb^{2+} (9), Fe^{3+} (10), Co^{2+} (11), K^{+} (12), Na^{+} (13), λ_{ex}=300 nm, λ_{em}=450 nm

addition of Zn^{2+} with the appearance of a new band at 360 nm which gradually increases up to 40 equiv. Zn^{2+} with a clear isosbestic point at 385 nm, implying the formation of SALTM- Zn^{2+} adduct. The changes of absorbance have been recorded up to 800 μM Zn^{2+} (Fig. 20). The linearity is observed up to 100 μM Zn^{2+}, useful for determination of unknown Zn^{2+} concentration.

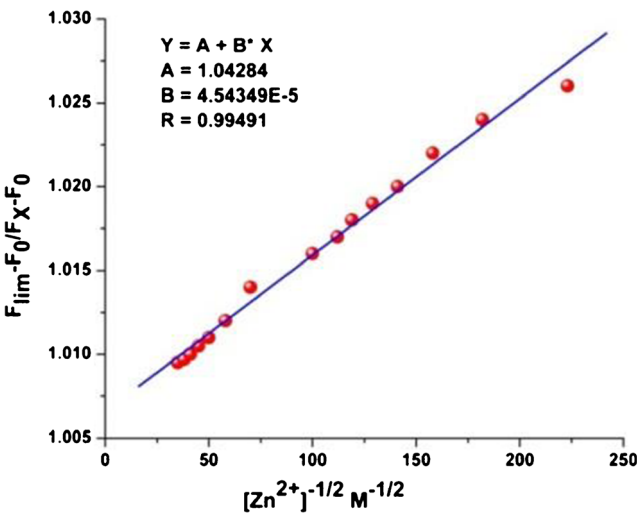

Fig. 17 Binding constant of SALTM for Zn^{2+} (Benesi-Hildebrand method)

Computational Studies

To rationalize the photo-physical properties of SALTM and its Zn^{2+} adduct, density functional theoretical (DFT) calculations have been performed using 6-31++G (d, p) and LANL2DZ basis sets. No significant difference between the results of two

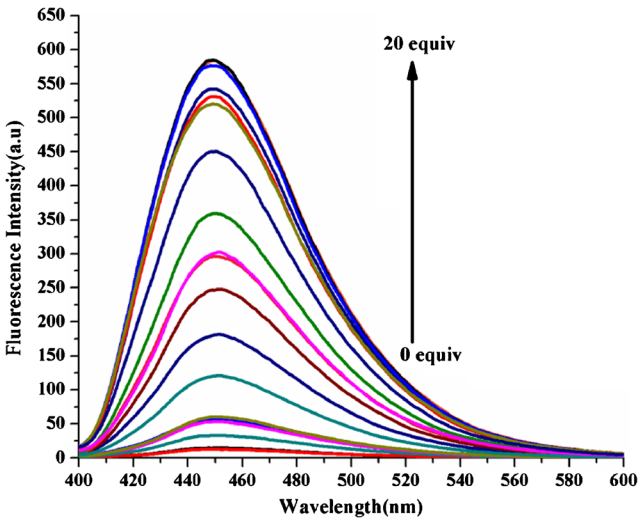

Fig. 18 Changes in the emission spectra of HNTM (20 μM) in HEPES buffered solution (ethanol: water,1:1, *v/v*, pH 7.4) upon gradual addition of Zn^{2+} (0.10, 0.2, 0.5, 1.0, 2.0, 3.0, 4.0, 5.0, 6.0, 7.0, 8.0, 9.0, 10.0, 25.0, 50.0, 100.0, 150,200, 250, 300, 350 and 400.0 μM) (λ_{ex}=380 nm)

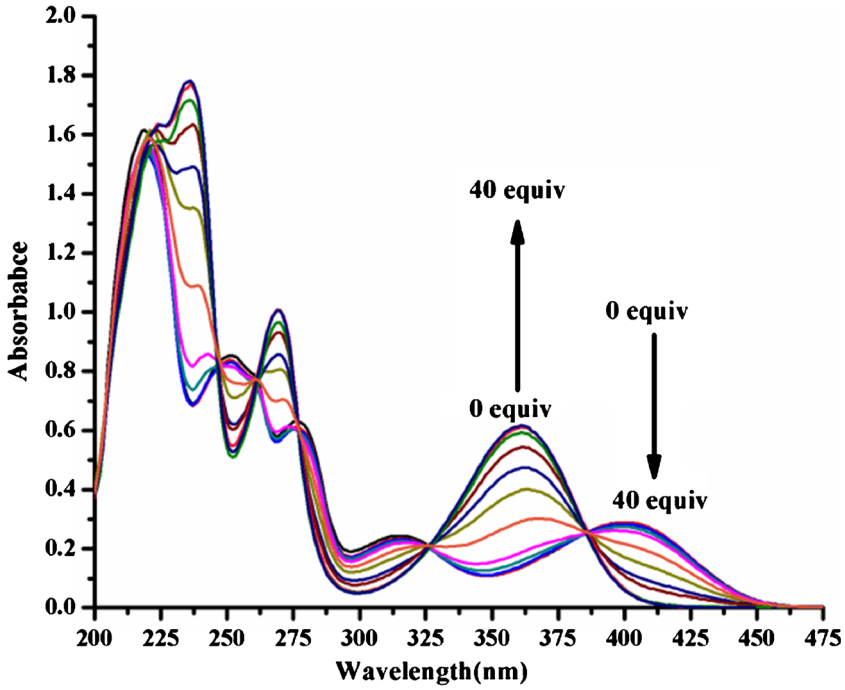

Fig. 19 Changes of absorbance of SALTM (20 μM) upon addition of Zn^{2+} (0.1, 0.2, 0.5, 1.0, 2.0, 3.0, 4.0, 5.0, 6.0, 7.0, 8.0, 9.0, 10.0, 25.0, 50.0, 100.0, 200.0, 400.0, 600.0 and 800.0 μM) in 100 % water at pH 7.4

methods has been observed. However, for SALTM-Zn^{2+} adduct, LANL2DZ basis set is used. The optimized geometries of SALTM and its Zn^{2+} adduct are shown in Fig. 21. TD-DFT studies provide deeper insight of emission properties of SALTM upon interaction with Zn^{2+}. Absorbance spectrum of aqueous solution of SALTM shows four bands centered at 405, 313, 276 and 251 nm.

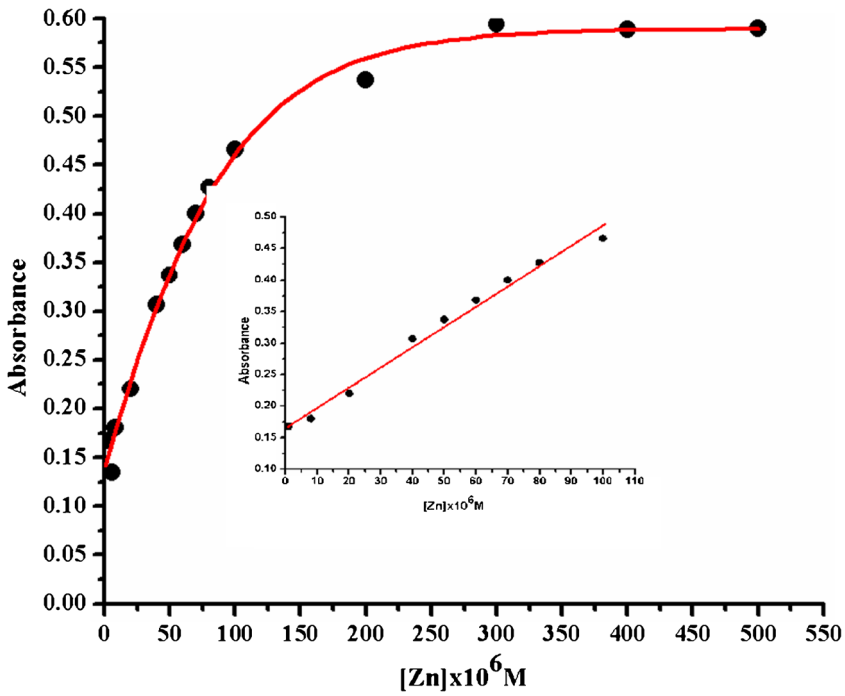

Fig. 20 Variation of absorbance of SALTM in 100 % water at pH 7.4 (300 nm) as a function of externally added Zn^{2+} (0.1–800.0 μM)

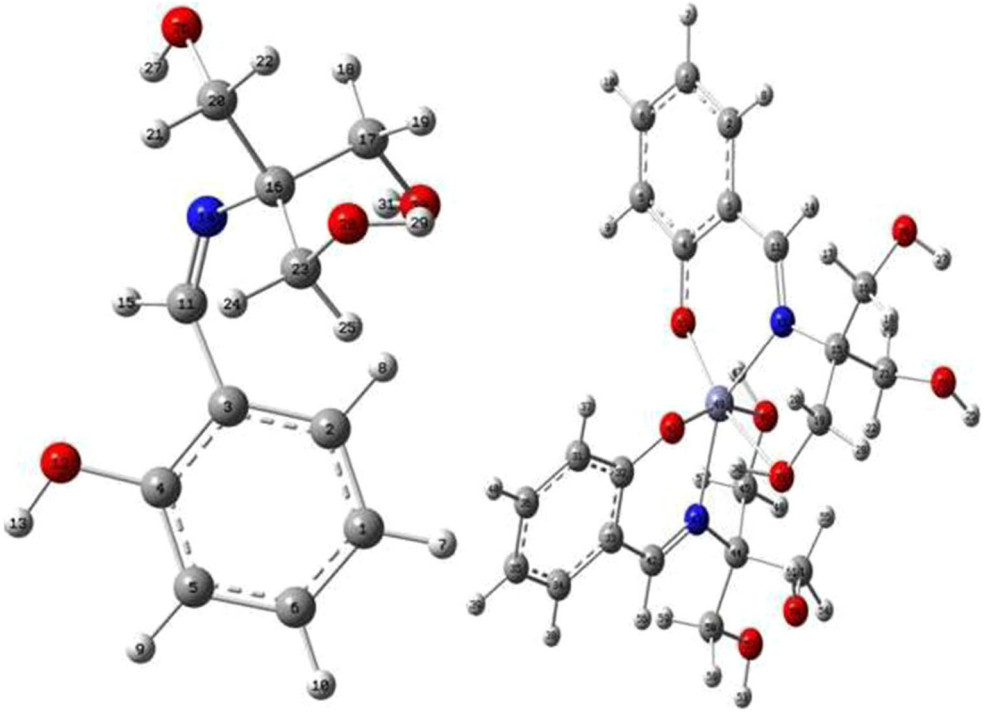

Fig. 21 Energy optimized structures of SALTM and its Zn^{2+} adduct

Table 7 indicates that HOMO to LUMO (oscillator strength, f=0.1559) and HOMO-2 to LUMO (f= 0.1398) are allowed transitions for SALTM (Fig. 22) involving emissions at 284 nm and 251 nm. This is in close agreement to experimental findings. Upon addition of Zn^{2+} to the aqueous solution of SALTM, the above mentioned bands disappear with the appearance of two new bands at 360 nm and 269 nm. Computational studies on [Zn^{2+}- (SALTM-H)] complex predicts allowable transition from HOMO −4 to LUMO (f= 0.2407) and HOMO −2 to LUMO +1 (f=0.40401) (Fig. 23) (Table 8) with emission wavelengths at 354 and 267 nm. Thus, theoretical studies are in line with the blue shift of emission band of SALTM in presence of Zn^{2+}.

HeLa Cell Imaging

Fresh media is supplemented with Zn^{2+} and SALTM accordingly and the cells are incubated for 2 h to facilitate Zn^{2+} or SALTM uptake. After incubation, cells are observed under an inverted fluorescence microscope (Dewinter, Italy) at different magnifications with UV filter. SALTM is then added to Zn^{2+} treated

Table 7 Electronic transitions observed from TDDFT studies of SALTM

Electronic transition	MOs involved	CI	Excitation energy/Wavelength,nm	Oscillator strength (f)
$S_0 \rightarrow S_1$	HOMO-2→LUMO	−0.1083	4.1568 eV/298 nm	0.0017
	HOMO-1→LUMO	0.6566		
	HOMO-1→LUMO+2	−0.1077		
$S_0 \rightarrow S_2$	HOMO-2→LUMO+1	0.1193	4.3585 eV/284 nm	0.1559
	HOMO→LUMO	0.6546		
$S_0 \rightarrow S_3$	HOMO-3→LUMO	0.1449	4.9407 eV/251 nm	0.1398
	HOMO-2→LUMO	0.6379		
	HOMO→LUMO+1	−0.13818		

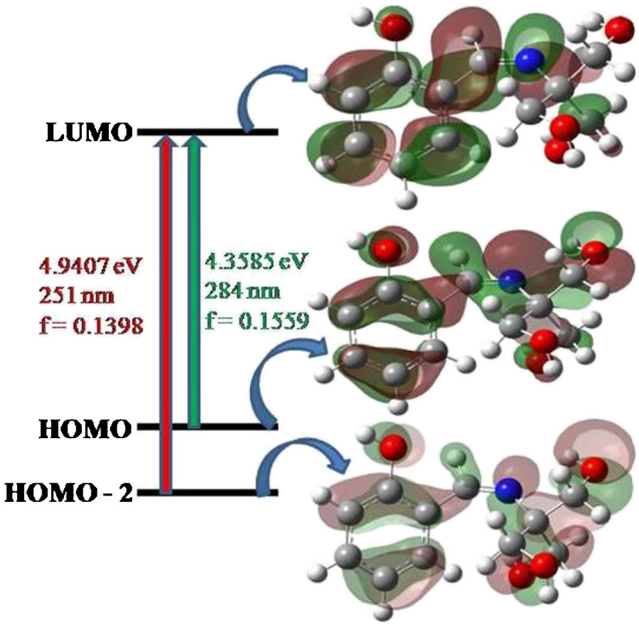

Fig. 22 Frontier molecular orbitals involved in the absorption spectrum of SALTM

cells and observed under microscope again. Images are recorded with an attached CCD camera equipped with Bio-Wizard 4.2 software (Fig. 24).

MTT assay has been performed to check the toxicity of the probe to the living cells. Figure 25 clearly indicates that significant numbers of in vitro cells are alive under the experimental conditions (cell imaging requires maximum 2.5 h whereas MTT assay have been performed after 48 h) in presence of the probe. The fluorescence cell imaging has been performed using excitation wavelength, 370 nm.

Conclusion

Two new Zn^{2+} selective fluorescence probes, viz. SALTM and HNTM have been reported. Both the probes are structurally characterized by single crystal X-ray analyses. SALTM functions in fully aqueous medium in a ratiometric manner while HNTM acts as a normal turn-on sensor in HEPES buffer medium. Moreover, SALTM may be easily and quickly synthesized in a single step from readily available starting materials. Zn^{2+} assisted CHEF of SALTM is attributed to the inhibition of CH=N isomerization leading to enhanced rigidity of the system. High water solubility of the probe makes it a potential candidate for biological Zn^{2+} monitoring in HeLa cancer cell. MTT assay suggests non-harmful nature of the probe towards living cell. The lowest LOD and binding constant of the probe for Zn^{2+} are quite satisfactory.

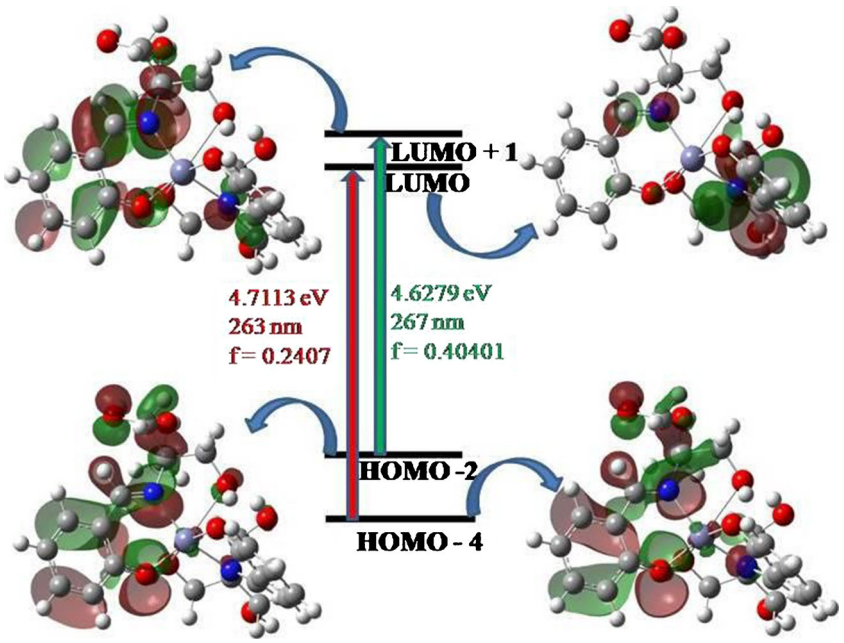

Fig. 23 Frontier molecular orbitals involved for the absorption of [Zn^{2+}- (SALTM-H)] adduct

Table 8 Electronic transitions observed from TDDFT studies of [SALTM-Zn^{2+}] complex

Electronic transition	Composition	CI	Excitation energy/Wavelength,nm	Oscillator strength (f)
$S_0 \rightarrow S_1$	HOMO→LUMO HOMO→LUMO+1	0.65560 0.10203	3.4970 eV/354 nm	0.0737
$S_0 \rightarrow S_8$	HOMO-3→LUMO+1 HOMO-2→LUMO+1	0.17930 0.40401	4.6279 eV/267 nm	0.2153
$S_0 \rightarrow S_{10}$	HOMO-4→LUMO HOMO-3→LUMO HOMO −5→LUMO+1	0.45499 0.28738 0.14883	4.7113 eV/263 nm	0.2407

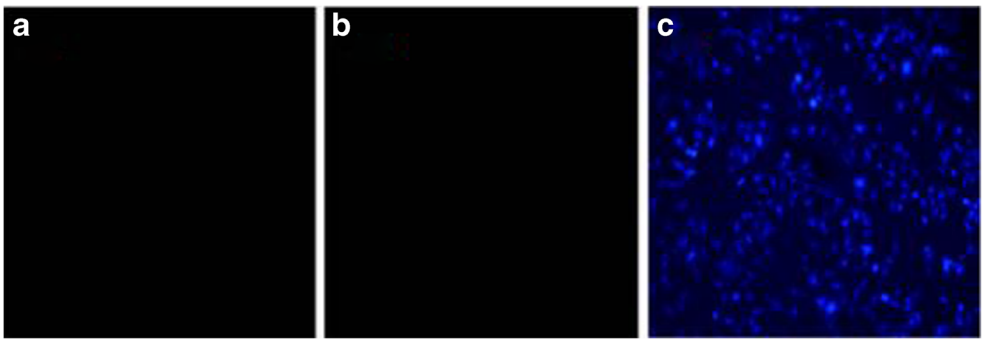

Fig. 24 Fluorescence microscope images of HeLa cells: **a** and **b** are images after incubation with Zn^{2+} (20 μM) and SALTM (20 μM) respectively. **c** Cells incubated with Zn^{2+} (20 μM) followed by addition of SALTM (20 μM, λ_{ex}=370 nm)

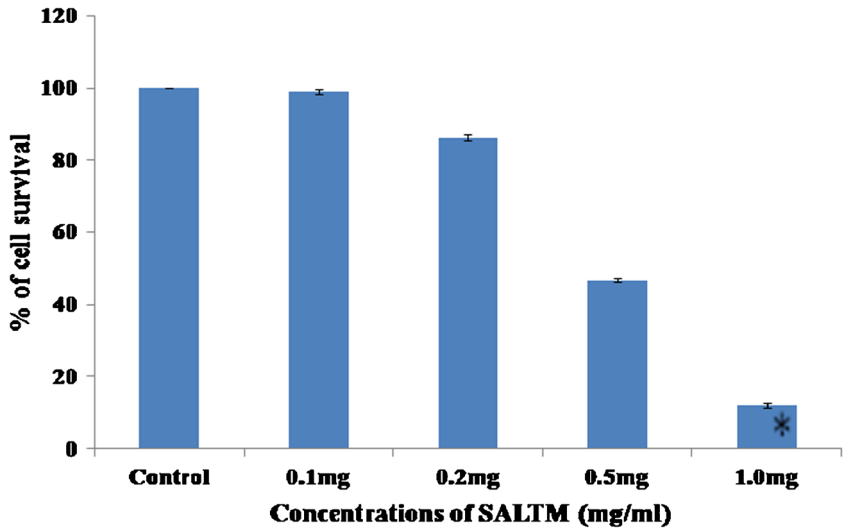

Fig. 25 MTT assay of HeLa cells after treatment with SALTM at different concentration for 48 h; for **1**, *$p<0.05$ significantly different

Acknowledgments B. Kumari and S. Lohar are thankful to BU and CSIR for fellowship. Assistance from CAS (UGC) is gratefully acknowledged.

References

1. Frederickson CJ, Koh JY, Bush AI (2005) The neurobiology of zinc in health and disease. Nat Rev Neurosci 6:449–462
2. Que EL, Domaille DW, Chang CJ (2008) Metals in neurobiology: probing their chemistry and biology with molecular imaging. Chem Rev 108:1517–1549
3. Lippard SJ, Berg JM (1994) Principles of bioinorganic chemistry. University Science, Mill Valley
4. Berg JM, Shi Y (1996) Galvanization of biology: a growing appreciation for the roles of zinc. Science 271:1081–1085
5. Auld DS (2001) Zinc coordination sphere in biochemical zinc sites. Biol Met 14:271–313
6. Wu ZK, Zhang YF, Ma JS, Yang GQ (2006) Ratiometric Zn^{2+} sensor and strategy for Hg^{2+} selective recognition by central metal ion replacement. Inorg Chem 45:3140–3142
7. Assaf SY, Chung SH (1984) Release of endogenous Zn2+ from brain tissue during activity. Nature 308:734–736
8. Howell GA, Welch MG, Frederickson CJ (1984) Stimulation-induced uptake and release of zinc in hippocampalslices. Nature 308:736–738
9. O'Halloran TV (1993) Transition metals in control of gene expression. Science 261:715–725
10. Koh JY, Suh SW, Gwag BJ, He YY, Hsu CY, Choi DW (1996) The role of zinc in selective neuronal death after transient global cerebral ischemia. Science 272:1013–1016
11. Suh SW, Jensen KB, Jensen MS, Silva DS, Kesslak PJ, Danscher G, Frederickson CJ (2000) Histochemically-reactive zinc in amyloid plaques, angiopathy, and degenerating neurons of Alzheimer's diseased brains. Brain Res 2000(852):274–278
12. Frederickson CJ, Bush AI (2003) Synaptically released zinc: physiological functions and pathological effects. BioMetals 14:353–366
13. Qian WJ, Gee KR, Kennedy RT (2003) Imaging of Zn^{2+} release from pancreatic beta-cells at the level of single exocytotic events. Anal Chem 75:3468–3475
14. Tomat E, Lippard SJ (2010) Imaging mobile zinc in biology. Curr Opin Chem Biol 14:225–230
15. Lim NC, Freake HC, Brückner C (2005) Illuminating zinc in biological systems. Chem Eur J 11:38–49
16. Dai Z, Canary JW (2007) Tailoring tripodal ligands for zinc sensing. New J Chem 31:1708
17. Xu Z, Yoon J, Spring DR (1996) Fluorescent chemosensors for Zn $^{2+}$. Chem Soc Rev 39:1996–2006
18. Lee HG, Lee JH, Jang SP, Park HM, Kim S, Kim Y, Kim C, Harrison RG (2011) Tetrahedron 67:8073
19. Sturgeon RE, Berman SS, Desaulniers A, Russell DS (1979) Determination of iron, manganese, and zinc in seawater by graphite furnace atomic absorption spectrometry. Anal Chem 51:2364–2369
20. Tang B, Huang H, Xu K, Tong L, Yang G, Liu X, An L (2006) Highly sensitive and selective near-infrared fluorescent probe for zinc and its application to macrophage cells. Chem Commun 34: 3609–3611
21. Atilgan S, Ozdemir T, Akkaya EU (2008) A sensitive and selective ratiometric near IR fluorescent probe for zinc ions based on the distyryl−bodipy fluorophore. Org Lett 10:4065–4067
22. Han ZX, Zhang XB, Li Z, Gong YJ, Wu XY, Jin Z, He CM, Jian LX, Zhang J, Shen GL, Yu RQ (2010) Efficient fluorescence resonance energy transfer-based ratiometric fluorescent cellular imaging probe for Zn^{2+} using a rhodaminespirolactam as a trigger. Anal Chem 82:3108–3113
23. Xu Y, Pang Y (2010) Zinc binding-induced near-IR emission from excited-state intramolecular proton transfer of abis(benzoxazole) derivative. Chem Commun 46:4070–4072
24. Zhu J, Yuan H, Chan W, Lee AWM (2010) A colorimetric and fluorescent turn-on chemosensor operative in aqueous media for Zn^{2+} based on a multi-functionalized spirobenzopyran derivative. Org Biomol Chem 8:3957–3964
25. Zhang Y, Guo XF, Si WX, Jia JH, Qian XH (2008) Ratiometric and water-soluble fluorescent zinc sensor of carboxamidoquinoline with an alkoxyethylamino chain as receptor. Org Lett 2008(10): 473–476
26. Ajayaghosh A, Carol P, Sreejith S (2005) A ratiometric fluorescence probe for selective visual sensing of Zn^{2+}. J Am Chem Soc 127:14962–14963
27. Akkaya EU, Huston ME, Czarnik AW (1990) Chelation-enhanced fluorescence of anthrylazamacrocycle conjugate probes in aqueous solution. J Am Chem Soc 112:3590–3593
28. Burdette SC, Frederickson CJ, Bu W, Lippard SJ (2003) ZP4, an improved neuronal Zn^{2+} sensor of the Zinpyr family. J Am Chem Soc 125:1778–1787
29. Ding Y, Xie Y, Li X, Hill JP, Zhang W, Zhu W (2011) Selective and sensitive "turn-on" fluorescent Zn^{2+} sensors based on di- and tripyrrins with readily modulated emission wavelengths. Chem Commun 47:5431–5433
30. Maity D, Govindaraju T (2012) A differentially selective sensor with fluorescence turn-on response to Zn^{2+} and dual-mode ratiometric response to Al^{3+} in aqueous media. Chem Commun 48:1039–1041
31. Xu Z, Liu X, Pan J, Spring DR (2012) Coumarin-derived transformable fluorescent sensor for Zn^{2+}. Chem Commun 48:4764–4766
32. Jiang J, Jiang H, Tang X, Yang L, Dou W, Liu W, Fang R, Liu W (2011) An efficient sensor for Zn^{2+} and Cu^{2+} based on different binding modes. Dalton Trans 40:6367–6370
33. Xu Z, Yoon J, Spring DR (2010) Fluorescent chemosensors for Zn^{2+}. Chem Soc Rev 39:1996–2006
34. Xu Y, Meng J, Meng L, Dong Y, Cheng Y, Zhu C (2010) A highly selective fluorescence-based polymer sensor incorporating an (R, R)-salen moiety for Zn^{2+} detection. Chem Eur J 16:12898
35. Liu X, Zhang N, Zhou J, Chang T, Fang C, Shangguan D (2013) A turn-on fluorescent sensor for zinc and cadmium ions based on perylene tetracarboxylic diimide. Analyst 138:901–906
36. Mikata Y, Yamashita A, Kawata K, Konno H, Itami S, Yasuda K, Tamotsu S (2012) Hydrogen liberation from the hydrolytic dehydrogenation of dimethylamine–borane at room temperature by using a novel ruthenium nano-catalyst. Dalton Trans 41:4976–4984
37. Parkesh R, Lee TC, Gunnlaugsson T (2007) Highly selective 4-amino-1,8-naphthalimide based fluorescent photo-induced electron transfer(PET) chemosensors for Zn(II) under physiological pH conditions. Org Biomol Chem 5:310–317
38. Wang L, Qin W, Liu W (2010) Synthesis, characterization and crystal structure of a new fluorescent probe based on Schiff Base for the detection of Zinc (II). Inorg Chem Commun 13:1122
39. Udhayakumari D, Saravanamoorthy S, Ashok M, Velmathi S (2011) Simple imine linked colorimetric and fluorescent receptor for sensing Zn^{2+} ions in aqueous medium based on inhibition of ESIPT mechanism. Tetrahedron Lett 52:4631–4635
40. Dong Y, Li J, Jiang X, Song F, Cheng Y, Zhu C (2011) Na^{+} triggered fluorescence sensors for Mg^{2+} detection based on a coumarin salen moiety. Org Lett 13:2252–2255
41. Cozzi PG (2004) Metal–Salen Schiff base complexes in catalysis: practical aspects. Chem Soc Rev 33:410–421
42. Pucci D, Aiello I, Bellusci A, Crispini A, Ghedini M, Deda ML (2009) Coordination induction of nonlinear molecular shape in

mesomorphic and luminescent Zn^{II} complexes based on salen-like frameworks. Eur J Inorg Chem 28:4274–4281
43. Niu LY, Guan YS, Chen YZ, Wu LZ, Tung CH, Yang QZ (2012) BODIPY-based ratiometric fluorescent sensor for highly selective detection of glutathione over cysteine and homocysteine. J Am Chem Soc 134:18928–18931
44. Das P, Mandal AK, Chandar AB, Baidya M, Bhatt HB, Ganguly B, Ghosh SK, Das A (2012) New chemo-dosimetric reagents as ratiometric probes for cysteine and homocysteine and possible detection in living cells and in blood plasma. Chem Eur J 18:15382–15393
45. Lin HY, Cheng PY, Wan CF, Wu AT (2012) A turn-on and reversible fluorescence sensor for zinc ion. Analyst 137:4415–4417
46. Ashton TD, Jolliffe KA, Pfeffer FM (2015) Luminescent probes for the bioimaging of small anionic species *in vitro* and *in vivo*. Chem Soc Rev 44:4547–4595
47. Woo H, You Y, Kim T, Jhon GJ, Nam W (2012) Fluorescence ratiometric zinc sensors based on controlled energy transfer. J Mater Chem 22:17100–17112
48. Burla MC, Caliandro R, Camalli M, Carrozzini B, Cascarano GL, Caro LD, Giacovazzo C, Polidori G, Spagna R (2005) SIR 2004: an improved tool for crystal structure determination and refinement. J Appl Crystallogr 38:381–388
49. Sheldrick GM (2008) A short history of SHELX. Acta Crystallogr Sect A 64:112–122
50. Banerjee A, Sahana A, Lohar S, Sarkar B, Mukhopadhyay SK, Das D (2013) A FRET operated sensor for intracellular pH mapping: strategically improved efficiency on moving from an anthracene to a naphthalene derivative. RSC Adv 3:14397–14405
51. Austin E, Gouterman M (1978) Absorption and emission of weak complexes with acids, bases, and salts. Bioinorg Chem 9:281–298
52. Melhuish WH (1961) Quantum efficiencies of fluorescence of organic substances: effect of solvent and concentration of the fluorescent solute. J Phys Chem 65:229–235
53. Reja SI, Bhalla V, Sharma A, Kaur G, Kumar M (2014) A highly selective fluorescent probe for hypochlorite and its endogenous imaging in living cells. Chem Commun 50:11911–11914
54. Benesi HA, Hildebrand JH (1949) A spectrophotometric investigation of the interaction of iodine with aromatic hydrocarbons. J Am Chem Soc 71:2703–2707